Pulsed Bessel–Gauss beams: a depleted wave model for type II second-harmonic generation

Mohammad Sabaeian,* Alireza Motazedian, Mostafa Mohammad Rezaee, and Fatemeh Sedaghat Jalil-Abadi

Department of Physics, Faculty of Science, Shahid Chamran University of Ahvaz, Ahvaz, Iran

*Corresponding author: sabaeian@scu.ac.ir

Received 4 August 2014; revised 9 October 2014; accepted 9 October 2014;
posted 10 October 2014 (Doc. ID 220331); published 5 November 2014

In this work, a three-dimensional and time-dependent nonlinear wave model to describe the generation of pulsed Bessel–Gauss second-harmonic waves (SHWs) is presented. Three coupled equations, two for ordinary and extraordinary fundamental waves and one for extraordinary SHWs, describing type II second-harmonic generation (SHG) in a $KTiOPO_4$ (KTP) crystal were solved by considering the depletion of fundamental waves (FWs). The results examined the validity of nondepleted wave approximation against the energy of pulses, beam spot size, and interaction length. It was shown that for pulses with spot sizes of $\omega_f = 80$ μm and energy of 0.8*j*, the nonlinear interaction was accomplished over a distance of ~5 mm. Therefore, for KTP crystals with lengths longer than 5 mm, the nondepleted wave approximation can no longer be valid. To be valid, the crystal must be shorter than the interaction length, i.e., 5 mm.

OCIS codes: (140.3460) Lasers; (190.0190) Nonlinear optics; (140.3538) Lasers, pulsed.
http://dx.doi.org/10.1364/AO.53.007691

1. Introduction

Bessel beams were first introduced by Durnin in 1987 [1]. These types of beams, theoretically, extend transversally toward infinity so that they carry an infinite amount of energy. Therefore, they were not physically meaningful and could not be generated experimentally. Hence, their transverse profile was accompanied with other profiles in order to carry a finite amount of energy. A profile restricting and dropping relatively quickly the transverse extension was a Gaussian profile. Thereby, the generated beam was called a Bessel–Gauss beam [2]. Among the potential applications of Bessel–Gauss beams, one can name transporting information [3], trapping particles and being used as optical tweezers [4,5], optical manipulating of micrometer-size nonorganic particles [6], and nonlinear optical processes [7–9]. One of the recent applications of Bessel–Gauss beams concerns the generation of the second harmonic of near-infrared light through the nonlinear optical processes. The importance of the green light emerges from the wide applications in spectroscopy [10], ophthalmology [11], pumping source of solid-state lasers [12], ocean exploration [13], laser probes [13], and underwater communication [13,14].

One of the most famous crystals that is being used for frequency conversion is potassium titanyl phosphate ($KTiOPO_4$), which is also abbreviated as KTP. This crystal possesses a high nonlinear conversion coefficient, wide acceptance angle, high thermal conductivity, small walking-off angle, and a relatively high damage threshold, making it suitable to convert the fundamental beam of 1064 nm to green light of 532 nm.

Second-harmonic beams have been generated using Bessel–Gauss beams [15,16]. Nevertheless, fewer works can be found, in particular, from the modeling point of view. Arlt *et al.* have investigated the efficiency of second-harmonic generation (SHG) by using Bessel–Gauss beams [17]. They have employed

1559-128X/14/327691-06$15.00/0

one-dimensional equations of SHG for LiB_3O_5 (LBO) crystal with type I phase matching, regardless of optical absorption. They also ignored the birefringence and anisotropy of the nonlinear crystal. The model was then solved numerically. Considering thermal effects, Sabaeian *et al.* presented a model for continuous wave (CW) Gaussian beam type II SHG in a single-pass cavity [18]. They coupled the second-harmonic equations with the heat and the mismatched phase equations. In that work, the sum frequency generation approach was employed to couple three nonlinear equations in a type II phase matching configuration. Recently, this model had been employed to enhance the nonlinear conversion efficiency experimentally [19]. More recently, the double-pass version of this model, including thermal effects, has been reported regenerating experimental data [20].

The present work aims to model and solve a depleted wave model describing the SHG with pulsed Bessel–Gauss beams. The sum frequency generation approach developed previously by Sabaeian *et al.* is used without considering the thermal effects. The coupled model considers the depletion of fundamental beams as well as the second-harmonic beam within a type II configuration in which two orthogonal polarized fundamental beams with equal frequencies are irradiated normally onto a KTP crystal, i.e., one polarization along the ordinary and another along the extraordinary direction. The resultant second-harmonic wave (SHW) would be phase matched along the extraordinary direction. Since finding the analytical solutions for these coupled equations when the Bessel–Gauss beams are used is a complex task and since, to the best of our knowledge, no analytical approach has been reported so far, a numerical procedure is adopted. As we will show, a quick depletion of fundamental beam amplitude/intensity due to its conversion into the SHW does not allow us to use a nondepleted wave approximation, although its usage may lead to a very simple mathematical treatment. In nondepleted approximation, it is assumed that the intensity/amplitude of FW over the crystal length is high enough, and it remains constant so that the SHW equation can be decoupled from two others and solved separately to describe the process of SHG. Although a nondepleted assumption for FW may be fulfilled for CW SHG due to a large interaction length [20], for pulsed SHG in which the peak power of the FW is much higher than that of CW, the smallness of the interaction length makes a complete energy conversion and so does not allow a nondepletion wave model to be valid any longer. Therefore, to solve the coupled equation, we use a numerical method. To this end, a homemade code was written in Intel Fortran and run in the Linux Ubuntu operating system. To avoid the detrimental thermal effects [18], low input powers are used to keep the heat load at its minimum level. The coupled equations were solved in the cylindrical coordinates to use the advantage of azimuthal symmetry of FW and SHW profiles; that is, the differential equations depend only on two coordinates of r and z and, of course, on t. As the Bessel–Gauss beams possess many more fluctuations in the radial direction compared to ordinary Gaussian beams, fine meshes were needed for convergence in the numerical treatment and to reach a stable and accurate solution. Huge contrivances were made to provide the capability of running the code with home-used computing machines.

2. Theory

In the paraxial wave approximation, in which $\partial^2 E/\partial z^2 \ll k\partial E/\partial z$, the wave equation consisting of the nonlinear source term is given by [21]

$$\frac{dE_n(r,z)}{dz} - \frac{i}{2k_n}\nabla_\perp^2 E_n(r,z) = \frac{i\omega_n}{2n\varepsilon_0 c}P_n^{Nl}(r,z), \qquad (1)$$

where $E_n(r,z)$ is the amplitude of electric field given by the relation of $E_n(r,z,t) = E_n(r,z)e^{i(k_n z-\omega_n t)} + \text{C.C.}$ And $k_n = n\omega_n/c$ is the wave number, with ω_n being the angular frequency, n being the refractive index, and c being the speed of the light. Since the pulsed beams are of interest in this work, a term of $\frac{n_n}{c}\frac{\partial E_n}{\partial t}$ is added on the left-hand side of Eq. (1) [21]. Considering the optical absorption of traveling waves, a term of $\gamma_n E_n/2$ is also added on the left-hand side of the field equation, where γ_n is the absorption coefficient.

Let us turn to the coupled equations. In the type II SHG in which two orthogonal fundamental beams with equal frequencies of $\omega_1 = \omega_2 = \omega$ generate a SHW with the frequency of $\omega_3 = \omega_1 + \omega_2 = 2\omega$, the coupled wave equations are given by [18]

$$\frac{n_1}{c}\frac{dE_1(r,z,t)}{dt} + \frac{dE_1(r,z,t)}{dz} + \frac{\gamma_1}{2}E_1(r,z,t) - \frac{ic}{2n_1\omega_1}\nabla_\perp^2\vec{E}_1(r,z,t) = \frac{2i\omega_1}{n_1 c}d_{\text{eff}}E_2^*(r,z,t)E_3(r,z,t)\exp(i\Delta kz), \qquad (2)$$

$$\frac{n_2}{c}\frac{dE_2(r,z,t)}{dt} + \frac{dE_2(r,z,t)}{dz} + \frac{\gamma_2}{2}E_2(r,z,t) - \frac{ic}{2n_2\omega_2}\nabla_\perp^2 E_2(r,z,t) = \frac{2i\omega_2}{n_2 c}d_{\text{eff}}E_1^*(r,z,t)E_3(r,z,t)\exp(i\Delta kz), \qquad (3)$$

$$\frac{n_3}{c}\frac{dE_3(r,z,t)}{dt} + \frac{dE_3(r,z,t)}{dz} + \frac{\gamma_3}{2}E_3(r,z,t) - \frac{ic}{2n_3\omega_3}\nabla_\perp^2 E_3(r,z,t) = \frac{2i\omega_3}{n_3 c}d_{\text{eff}}E_1(r,z,t)E_2(r,z,t)\exp(-i\Delta kz), \qquad (4)$$

where $\Delta k = (k_1 + k_2 - k_3)$ is the vector mismatching having a degradation effect on the SHG process. To provide the vector-matching condition, one can take advantage of the anisotropic properties of KTP crystal. Cutting the crystal with angles of $\theta = 90°$ and $\varphi = 22.7°$, the vector matching is established.

In order to reduce the errors in the numerical procedure, it is better to introduce some changes of variables as

$$\psi_1 = \frac{E_1}{\sqrt{P_1/2n_1c\varepsilon_0\pi\omega_f^2}} \Rightarrow |\psi_1|^2 = \frac{2n_1c\varepsilon_0|E_1|^2}{P_1/\pi\omega_f^2} = \frac{I_1}{I_1(0)}, \tag{5}$$

$$\psi_2 = \frac{E_2}{\sqrt{P_2/2n_2c\varepsilon_0\pi\omega_f^2}} \Rightarrow |\psi_2|^2 = \frac{2n_2c\varepsilon_0|E_2|^2}{P_2/\pi\omega_f^2} = \frac{I_2}{I_2(0)}, \tag{6}$$

$$\psi_3 = \frac{E_3}{\sqrt{P_3/n_3c\varepsilon_0\pi\omega_f^2}} \Rightarrow |\psi_3|^2 = \frac{n_3c\varepsilon_0|E_3|^2}{P_3/\pi\omega_f^2} = \frac{I_3}{I_3(0)}. \tag{7}$$

Accordingly, $|\psi_1|^2$ gives the efficiency of ordinary FW, $|\psi_2|^2$ the efficiency of extraordinary FW, and $|\psi_2|^2$ the efficiency of extraordinary SHW. Using the change of variables given above and cylindrical coordinates, three coupled wave equations take the form of

$$\frac{n_1}{c}\frac{d\psi_1}{dt} + \frac{d\psi_1}{dz} + \frac{\gamma_1}{2}\psi_1 - \frac{ic}{2n_1\omega}\frac{1}{r}\frac{d\psi_1}{dr} - \frac{ic}{2n_1\omega}\frac{d^2\psi_1}{dr^2} = \frac{i}{L}\psi_2^*\psi_3, \tag{8}$$

$$\frac{n_2}{c}\frac{d\psi_2}{dt} + \frac{d\psi_2}{dz} + \frac{\gamma_2}{2}\psi_2 - \frac{ic}{2n_2\omega}\frac{1}{r}\frac{d\psi_2}{dr} - \frac{ic}{2n_2\omega}\frac{d^2\psi_2}{dr^2} = \frac{i}{L}\psi_1^*\psi_3, \tag{9}$$

$$\frac{n_3}{c}\frac{d\psi_2}{dt} + \frac{d\psi_3}{dz} + \frac{\gamma_3}{2}\psi_3 - \frac{ic}{4n_3\omega}\frac{1}{r}\frac{d\psi_3}{dr} - \frac{ic}{4n_3\omega}\frac{d^2\psi_3}{dr^2} = \frac{i}{L}\psi_1\psi_3, \tag{10}$$

where $L = \sqrt{n_1n_2n_3c^3\varepsilon_0\pi\omega_f^2/4P\omega^2d_{\text{eff}}^2}$ is the *interaction length*. This important quantity is a characteristic distance over which the fields exchange their energy. Equations (8)–(10) are in dimensionless forms, which are coupled together.

At the entrance face of the crystal, the Bessel–Gauss profiles for FWs are assumed as the boundary conditions. For SHW, we set $\psi_3(t, z = 0) = 0$. A Bessel function of zero order, $J_0(\alpha r)$, in which α is the transverse wave number, is of interest. Considering the time dependence of beams as a Gaussian function, the FWs at $z = 0$ read

$$\psi_{1,2}(t, r, z = 0) = \exp[-(t - 2t_p)^2/t_p^2] \times J_0(\alpha r) \times \exp(-r^2/\omega_f^2), \tag{11}$$

where we have shifted the time origin to $2t_p$ [22] so that $\psi_1(t = 0, r, z) = \psi_2(t = 0, r, z) \approx 0$. We choose $t_p = 50$ μs [22] as the duration time of pulses and $\alpha = 51532$ m^{-1} as the transverse wave vector. α is calculated according to the equation $\alpha = (2\pi/\lambda_1)\sin(\beta)$ with $\beta = 1°$ [23] as the cone angle of the axicon used in the Bessel–Gauss setups. ω_f is the beam spot size at the entrance face of crystal and is taken to be constant over the crystal length [18], because the crystal length is less than the Rayleigh range.

3. Results

The coupled equations of (8)–(10) were solved numerically by a finite difference method. A homemade code has been written in the Intel Fortran Compiler and run with a Linux operating system. The optical properties of crystal are as follows: $n^{o,\omega} = 1.8296$, $n^{e,\omega} = 1.7466$, $n^{e,2\omega} = 1.7881$, $\gamma_1 = \gamma_2 = 0.5$ m^{-1} for $\lambda_{1,2} = 1064$ nm, $\gamma_3 = 4$ m^{-1} for $\lambda_3 = 532$ nm, and $d_{\text{eff}} = 7.3$ pm/V [18]. A KTP crystal with length of 2 cm and radius of 2 mm was used. The results presented in Figs. 1–7 were calculated for a pulsed beam with a spot size of $\omega_f = 80$ μm and an energy of 0.8j, except for Fig. 8, where several energies have been used.

Figure 1 shows the FW efficiency along the crystal length in several times. From the bottom to the top for solid curves, the times are $t = 25$, 50, 75, and 100 μs, and from the top to the bottom for dashed curves, the times are $t = 125$, 150, 175, and 200 μs.

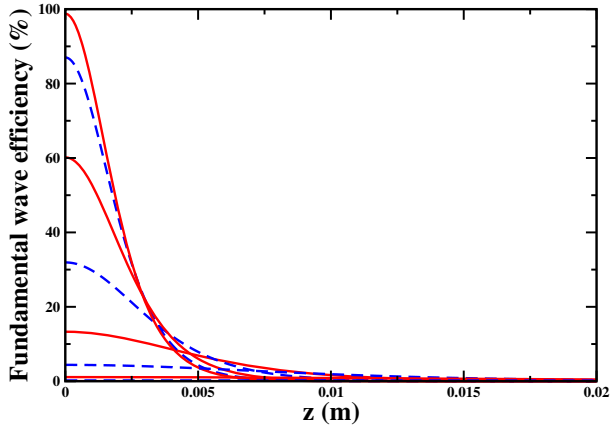

Fig. 1. Efficiency of the FW along the crystal axis for several times. From the bottom to the top, the solid curves are $t = 25$, 50, 75, and 100 μs. From the top to the bottom, the dashed curves are $t = 125$, 150, 175, and 200 μs.

As the figure shows, the fundamental field efficiency starts growing from zero at $t = 0$ and reaches 100% at $t = 2t_p$. It then starts dropping from 100% at $t = 100$ μs and reaches zero at $t = 200$ μs. The efficiency of the FW along the crystal length drops and approaches zero in a distance of ∼5 mm, whereas our crystal is 20 mm in length. This event proves that in this case the nondepleted wave approximation cannot be valid, since the FW loses its energy in a short distance compared to crystal length. The parameters chosen for the crystal and FWs, i.e., the crystal length, the beam spot size, and the energy, lead to a complete energy exchange over a short distance of crystal. To examine the validity of nondepleted approximation, one should note that the FW energy should be approximately constant over the crystal length so that the second-harmonic equation can be solved separately. The duration of the pulses in this work has been chosen to be somewhat long; that is, the microsecond pulses that are considered are assumed to be long pulses. Therefore, for shorter pulses such as nano, pico, or even femtosecond pulses, the situation becomes more critical since the nondepleted wave approximation loses its validity completely in a much shorter distance than 5 mm.

Figure 2 shows the SHW efficiency along the crystal length at different times, those chosen for FW in Fig. 1. Similar to previous cases, the solid curves show the increasing of the field, and the dashed curves show the decreasing of the field in time. According to this figure, the efficiency of SHW at $t = 2t_p$, after passing a distance of $z \simeq 5$ mm, reaches its maximum, which is 100%. Then it drops slightly due to the optical absorption of SHW in the crystal.

Figure 3 brings the SHW and FW efficiencies together along the crystal length at a time of $t = 2t_p$ at which the FW energy reaches its maximum. Two cases of considering the optical absorption of the waves (solid curve for fundamental wave and dashed curve for SHW) and ignoring the optical absorption of waves (dotted curve for fundamental wave and dashed-dotted curve for SHW) have been inspected. We have plotted two waves in a single figure to confirm the energy conservation and to check the numerical results. At a distance over which the FW vanishes (∼5 mm), the SHW saturates and receives all energy of FW. This event in reality cannot happen, due to thermal effects; however, as our main goal in this work is examining the nondepletion wave approximation, a 100% conversion efficiency is normal. With respect to the fact that the full energy exchange between the fundamental and SHWs completes at a distance of ∼5 mm much shorter than 20 mm of crystal length, one can conclude that for a crystal and the beam specifications used in this work, the depleted wave formalism is quite necessary. Therefore constant beam approximation for fundamental beams can no longer be correct. We should note here that the smaller the beam spot size, the shorter the resulting interaction length.

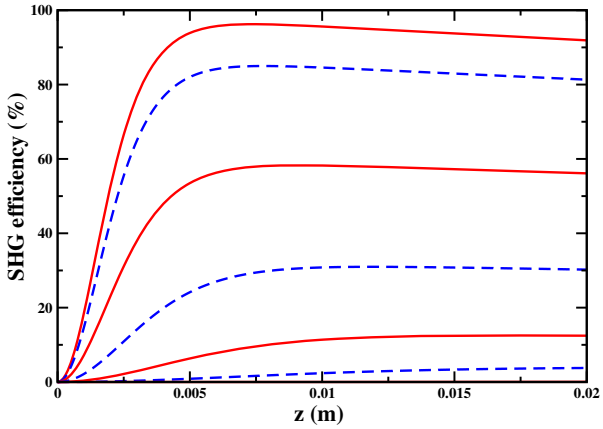

Fig. 2. Efficiency of the SHW along the crystal axis at several times as used in Fig. 1.

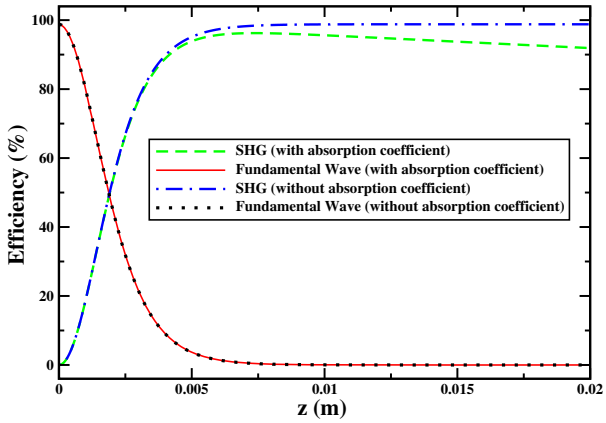

Fig. 3. Efficiency of SHG and FW along the crystal axis.

Figure 4 shows the efficiency of the FW along the radial distance at the input surface of the crystal ($z = 0$). The FW that is irradiated onto the crystal face possesses a Bessel–Gauss profile. The efficiency of this wave at the input face of the crystal, prior to the start of the energy exchange, is 100(%), where reduction is oscillatory toward the crystal circumstance. At the output face, Fig. 5, the FW efficiency is quite negligible and is about 0.5%. It is safe to say that a Bessel–Gauss SHW is generated in the crystal as a result of energy conversion, where its transverse profile at the end face of the crystal ($z = 2$ cm) is shown in Fig. 6. As can be seen from Fig. 6, the efficiency of SHW at the end face of the crystal reaches ∼90%, indicating a high level of energy conversion from FW to SHW.

Figure 7 shows the FW and SHW efficiencies versus the time at a point of $r = 0$ at the crystal end face. Accordingly, the FW (dashed curve) has given all its energy to SHW (solid curve) at all times.

In order to show how and where the nondepleted wave approximation loses its validity, we examined the SHG efficiency with changing the energy of pulses with the energies of 0.1, 0.2, 0.4, 0.6, 0.8, 1j, which are shown in Fig. 8. As the figure shows, the higher energy results in the smaller interaction length and thus a quicker energy exchange; that is, for higher energies, the exchange of energy between FW and SHW is accomplished in shorter distances.

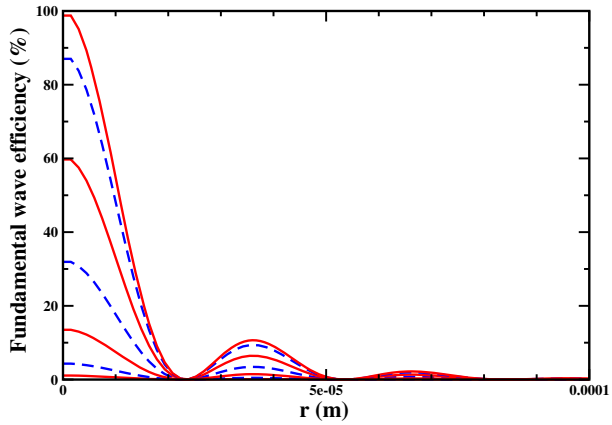

Fig. 4. Efficiency of FW in the radial direction for input surface of the crystal. Various curves correspond to several times as used in Fig. 1.

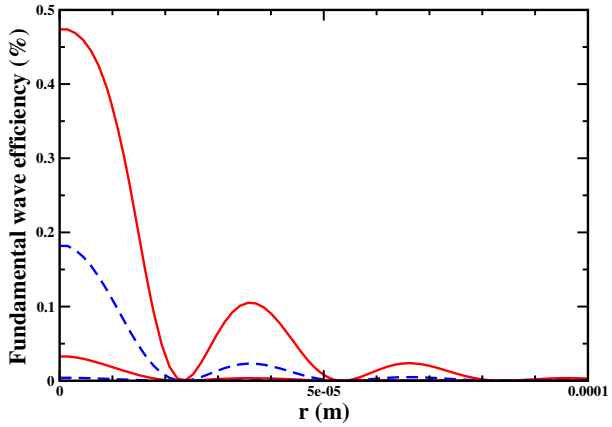

Fig. 5. Efficiency of FW in the radial direction at the output surface of the crystal.

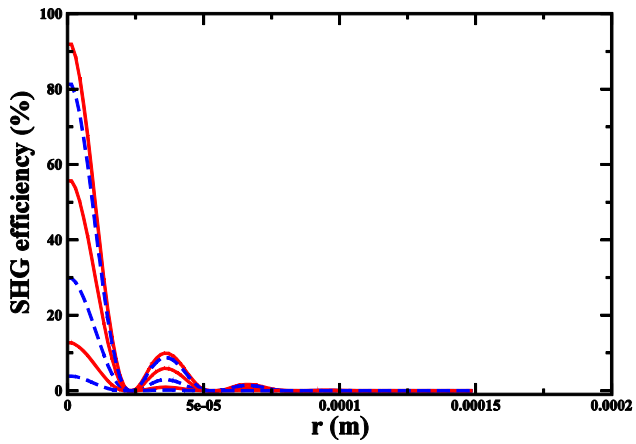

Fig. 6. Efficiency of SHG in the radial direction at the output surface of the crystal.

This can be understood from the relation of $L = \sqrt{n_1 n_2 n_3 c^3 \varepsilon_0 \pi \omega_f^2 / 4 P \omega^2 d_{\text{eff}}^2}$ determining the interaction length. The beam spot size appears in the nominator and FW power in the denominator. A quick

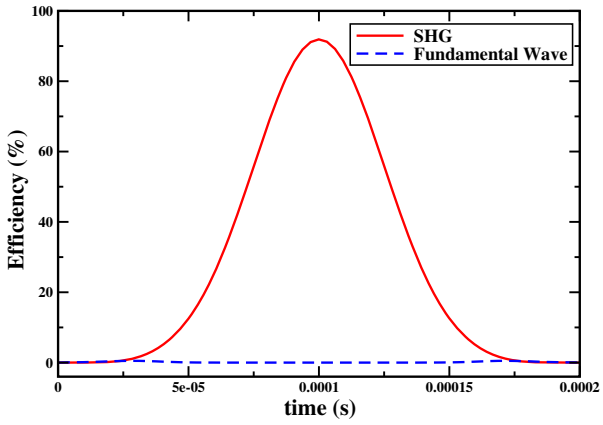

Fig. 7. Efficiency of FW (dashed curve) and SHW (solid curve) at the output face of the crystal.

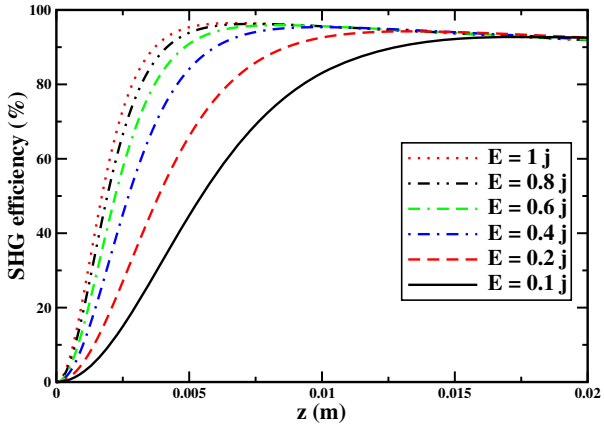

Fig. 8. Efficiency of SHW along the crystal axis for different energies.

glance at the curves represented in Fig. 8 shows that with increasing the pulse energy, the distance over which SHW grows shortens. For example, for $0.1j$ energy, the SHG process is completed in ~16 mm, whereas for $1j$ energy, it is completed in 5 mm. Since the energy parameter is presented inside the parentheses in the interaction length expression, the shortening of the interaction length with increasing pulse energy is not a linear event. Therefore, one can conclude that for the nondepleted wave approximation to be valid, the energy of the pulse should be lowered as much as possible. Other contrivances can be done with respect to the beam spot size. With enlarging the beam spot size, the fundamental beam intensity drops, and hence the interaction length becomes larger. Under this condition, the nondepleted wave approximation can be valid.

4. Conclusion

In this work, the coupled equations of pulsed SHG for type II configuration to generate the Bessel–Gauss beams were solved in the depleted wave model, and the validity of nondepleted wave approximation was examined in terms of beam energy and beam spot size. Since three waves, i.e., two ordinary and

extraordinary FWs and one extraordinary SHW, are interacting in the nonlinear crystal, the formalism of sum frequency generation developed in [18] was employed. Bessel–Gauss beams oscillate severely in the transverse plane compared to ordinary Gaussian waves. To achieve the more realistic results, optical absorption of FWs as well as the SHW were taken into account in the modeling. The results showed how pulsed Bessel–Gauss SHW is generated during the interaction of the waves and how much of the FW energy is exchanged along the crystal length. According to our results, for FW with energy of 0.8*j* and a beam spot size of 80 μm, the nonlinear interaction of waves is accomplished at a distance of ∼5 mm in a crystal with a length of 20 mm. Therefore, it seems that for such crystal and beam specifications, the nondepleted wave approximation is no longer valid. To be valid, a short crystal below 5 mm should be used. The reason behind such results can be found in the fact that for pulsed beams, the beam peak power is much higher than CWs so that the interaction length shortens. As discussed in Ref. [20], the efficiency of pulsed SHG is much higher than CW operation because of its short interaction length.

All calculations have been done using a homemade code written in Intel Fortran version 14.04 and were run in Linux operating system.

The authors would like to thank Shahid Chamran of the University of Ahvaz for supporting this work.

References

1. J. Durnin, "Exact solutions for nondiffracting beams. I. The scalar theory," J. Opt. Soc. Am. A **4**, 651–654 (1987).
2. F. Gori, G. Guattari, and C. Padovani, "Bessel–Gauss beams," Opt. Commun. **64**, 491–495 (1987).
3. M. A. Bandres, J. C. Gutiérrez-Vega, and S. Chávez-Cerda, "Parabolic nondiffracting optical wave fields," Opt. Lett. **29**, 44–46 (2004).
4. J. Fan, E. Parra, K. Kim, I. Alexeev, H. Milchberg, J. Cooley, and T. Antonsen, "Resonant self-trapping of high intensity Bessel beams in underdense plasmas," Phys. Rev. E **65**, 056408 (2002).
5. J. Arlt, V. Garces-Chavez, W. Sibbett, and K. Dholakia, "Optical micromanipulation using a Bessel light beam," Opt. Commun. **197**, 239–245 (2001).
6. D. McGloin, V. Garcés-Chávez, and K. Dholakia, "Interfering Bessel beams for optical micromanipulation," Opt. Lett. **28**, 657–659 (2003).
7. C. Conti and S. Trillo, "X waves generated at the second harmonic," Opt. Lett. **28**, 1251–1253 (2003).
8. V. Magni, "Optimum beams for efficient frequency mixing in crystals with second order nonlinearity," Opt. Commun. **184**, 245–255 (2000).
9. R. Gadonas, V. Jarutis, R. Paškauskas, V. Smilgevičius, A. Stabinis, and V. Vaičaitis, "Self-action of Bessel beam in nonlinear medium," Opt. Commun. **196**, 309–316 (2001).
10. Y. Lu, S. Huang, and Z. Sun, "Raman spectroscopy of phenylcarbyne polymer films under pulsed green laser irradiation," J. Appl. Phys. **87**, 945–951 (2000).
11. I. C. Frennesson and S. Nilsson, "Effects of argon (green) laser treatment of soft drusen in early age-related maculopathy: a 6 month prospective study," Br. J. Ophthalmol. **79**, 905–909 (1995).
12. M. Tsunekane, H. Inaba, and N. Taguchi, "High-power, efficient, low-noise, continuous-wave all-solid-state Ti:sapphire laser," Opt. Lett. **21**, 1912–1914 (1996).
13. D.-G. Xu, J.-Q. Yao, B.-G. Zhang, R. Zhou, E. Li, S.-Y. Zhao, X. Ding, W.-Q. Wen, Y.-X. Niu, and J. Hu, "110 W high stability green laser using type II phase matching $KTiOPO_4$(KTP) crystal with boundary temperature control," Opt. Commun. **245**, 341–347 (2005).
14. T. Wiener and S. Karp, "The role of blue/green laser systems in strategic submarine communications," IEEE Trans. Commun. **28**, 1602–1607 (1980).
15. S. Saltiel, W. Krolikowski, D. Neshev, and Y. S. Kivshar, "Generation of Bessel beams by parametric frequency doubling in annular nonlinear periodic structures," Opt. Express **15**, 4132–4138 (2007).
16. A. Piskarskas, V. Smilgevičius, A. Stabinis, V. Jarutis, V. Pašiškevičius, S. Wang, J. Tellefsen, and F. Laurell, "Noncollinear second-harmonic generation in periodically poled $KTiOPO_4$ excited by the Bessel beam," Opt. Lett. **24**, 1053–1055 (1999).
17. J. Arlt, K. Dholakia, L. Allen, and M. Padgett, "Efficiency of second-harmonic generation with Bessel beams," Phys. Rev. A **60**, 2438–2441 (1999).
18. M. Sabaeian, L. Mousave, and H. Nadgaran, "Investigation of thermally-induced phase mismatching in continuous-wave second harmonic generation: a theoretical model," Opt. Express **18**, 18732–18743 (2010).
19. K. Regelskis, J. Želudevičius, N. Gavrilin, and G. Račiukaitis, "Efficient second-harmonic generation of a broadband radiation by control of the temperature distribution along a nonlinear crystal," Opt. Express **20**, 28544–28556 (2012).
20. M. Sabaeian, F. S. Jalil-Abadi, M. Mohammad Rezaee, and A. Motazedian, "Heat coupled Gaussian continuous-wave double-pass type-II second harmonic generation: inclusion of thermally induced phase mismatching and thermal lensing," Opt. Express **22**, 25615–25628 (2014).
21. R. W. Boyd, *Nonlinear Optics* (Academic, 2003).
22. M. Sabaeian, "Analytical solutions for anisotropic time-dependent heat equations with Robin boundary condition for cubic-shaped solid-state laser crystals," Appl. Opt. **51**, 7150–7159 (2012).
23. S. Parsa, H. R. Fallah, M. Ramezani, and M. Soltanolkotabi, "Generation of pulsed Bessel–Gauss beams using passive axicon-theoretical and experimental studies," Appl. Opt. **51**, 7339–7344 (2012).